Proc. Int. Symp. "Brittle Matrix Composites 8"
A.M. Brandt, V.C. Li and I. H. Marshall, eds.
Warsaw, October 23-25, 2006
ZTUREK RSI and Woodhead Publ., Warsaw 2006

MODELLING OF METALLIC INTER-GRANULAR LAYERS IN POLYCRYSTALLINE CERAMICS

Eligiusz POSTEK[1)], Tomasz SADOWSKI[2)], Christophe DENIS[3)]
[1)] The University of Leeds, School of Earth and Environment,
Institute of Geophysics and Tectonics, Leeds, LS2 9JT, UK
e-mail: earewp@earth.leeds.ac.uk
[2)] Faculty of Civil and Sanitary Engineering, Department of Solid Mechanics,
Lublin University of Technology, ul. Nadbystrzycka 40, 20-618 Lublin, Poland
e-mail: tsadow@akropolis.pol.lublin.pl
[3)] University of Pierre et Marie Curie, Paris 6, CNRS UMR 7606,
Laboratory of Computer Sciences LIP6, 8 rue du Capitaine Scott, 75015 Paris, France
e-mail: christophe.denis@lip6.fr

ABSTRACT

The aim of the paper is to present a constitutive model for the case of uniaxial tension of the polycrystalline materials, including the inter-granular metallic layers that create its internal structure. The quasi-static deformation process of the material comprises elastic deformation of brittle grains, elasto-plastic deformation of intergranular layers and additional deformation due to micro-porosity development in layers. A Representative Volume Element (RVE) was analysed taking into consideration an initial internal structure of the material obtained from SEM photographs

Keywords
Ceramics, interfaces, finite strains

INTRODUCTION

A typical application of polycrystalline materials is the fabrication of cutting tools. The tools are working in such severe conditions as high dynamic and temperature loadings. An exemplary two-phase material used for them may consist of elastic grains and ductile interfaces. An example of SEM image showing grains, interfaces and their idealization are presented in Fig 1a and Fig 1b, respectively. The grains can exhibit anisotropic behaviour. The interfaces are thick enough not to be treated as only contacting adhesive layers. Our interest will focus on the behavior of the relatively thick intergranular layers which affect performance of entire sample. The interface material has different grades of porosity.

MATHEMATICAL FORMULATION

Incremental equation of equilibrium

The problem is elasto-plastic with the assumption of large displacements, [1-3]. We consider nonlinear terms of the strain tensor. The virtual work equation is of the form

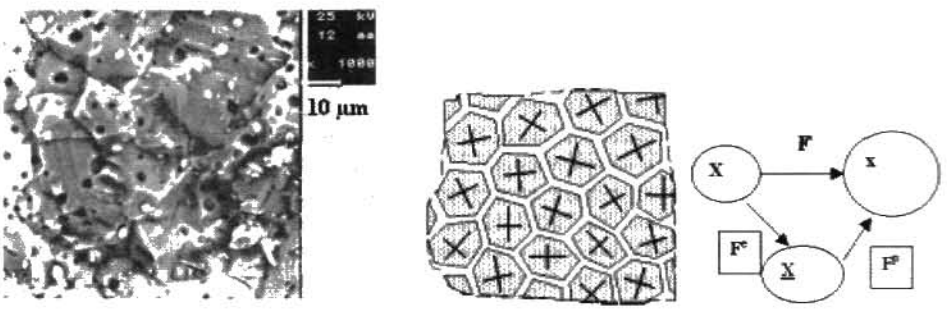

(a) (b) (c)

Figure 1. SEM image of a polycrystal (a), idealization (b). gradient decomposition into elastic and plastic parts (c)

$$\delta\Pi = \int_{\Omega^o} {}^{t+\Delta t}_{o}\mathbf{S} \cdot \delta\, {}^{t+\Delta t}_{o}\mathbf{E}\, d\Omega^o - \int_{\Omega^o} {}^{t+\Delta t}\mathbf{f}\,\delta^{t+\Delta t}\mathbf{u}\, d\Omega^o - \int_{\partial\Omega^o_\sigma} {}^{t+\Delta t}\mathbf{t}\,\delta^{t+\Delta t}\mathbf{u}\, d\left(\partial\Omega^o_\sigma\right) \tag{1}$$

where **S** and **E** are the II Piola-Kirchhof stress tensor and Green Lagrange strains, **f**, **t** and **u**={u,v,w} are body forces, boundary tractions and displacements. All of the quantities are determined at time t+Δt in the initial configuration. To obtain the above equation at time $t+\Delta t$ in the configuration at time t the relations [4], [5], are used

$${}^{t+\Delta t}_{o}\mathbf{S} = \frac{\rho}{\rho_o}\, {}^{t+\Delta t}_{t}\mathbf{S}, \quad {}^{t+\Delta t}_{o}\mathbf{E} = \frac{\rho}{\rho_o}\, {}^{t+\Delta t}_{t}\mathbf{E}, \quad \rho\, d\Omega^t = \rho_o\, d\Omega^o \tag{2}$$

$$\int_{\Omega^t} {}^{t+\Delta t}_{t}\mathbf{S} \cdot \delta\, {}^{t+\Delta t}_{t}\mathbf{E}\, d\Omega^t = \int_{\Omega^t} {}^{t+\Delta t}\mathbf{t}\,\delta^{t+\Delta t}\mathbf{u}\, d\Omega^t + \int_{\partial\Omega^t_\sigma} {}^{t+\Delta t}\mathbf{t}\,\delta^{t+\Delta t}\mathbf{u}\, d\left(\partial\Omega^t_\sigma\right) \tag{3}$$

Now, we apply incremental decomposition to the quantities in the equation above: strains, stresses, displacements and forces

$${}^{t+\Delta t}_{t}\mathbf{E} = {}^{t}_{t}\mathbf{E} + \Delta\mathbf{E}, \quad {}^{t+\Delta t}_{t}\mathbf{S} = {}^{t}_{t}\mathbf{S} + \Delta\mathbf{S}, \quad {}^{t+\Delta t}\mathbf{u} = {}^{t}\mathbf{u} + \Delta\mathbf{u}, \quad {}^{t+\Delta t}\mathbf{f} = {}^{t}\mathbf{f} + \Delta\mathbf{S}, \quad {}^{t+\Delta t}\mathbf{t} = {}^{t}\mathbf{t} + \Delta\mathbf{t} \tag{4}$$

Since the II P-K tensor at time t in the configuration t is equal to the Cauchy stress tensor the stress decomposition is of the form

$${}^{t}_{t}\mathbf{S} = {}^{t}_{t}\boldsymbol{\tau}, \qquad {}^{t+\Delta t}_{t}\mathbf{S} = {}^{t}_{t}\boldsymbol{\tau} + \Delta\mathbf{S} \tag{5}$$

Then, we employ the following strain increment decomposition into its linear and nonlinear parts in the following form

$$\Delta\mathbf{E} = \Delta\mathbf{e} + \Delta\boldsymbol{\eta}, \;\; \Delta\mathbf{e} = \overline{\mathbf{A}}\Delta\mathbf{u}, \;\; \Delta\boldsymbol{\eta} = \overline{\overline{\mathbf{A}}}(\Delta\mathbf{u}')\Delta\mathbf{u}'/2 \tag{6}$$

where $\Delta\mathbf{u}'$ is the vector of the displacement increment derivatives w.r.t. Cartesian coordinates and ($\overline{\mathbf{A}}$, $\overline{\overline{\mathbf{A}}}$) are the linear and nonlinear operators, [2].

$$\overline{\mathbf{A}} = \begin{bmatrix} \frac{\partial}{\partial x} & 0 & 0 \\ 0 & \frac{\partial}{\partial y} & 0 \\ 0 & 0 & \frac{\partial}{\partial z} \\ \frac{\partial}{\partial y} & \frac{\partial}{\partial x} & 0 \\ \frac{\partial}{\partial z} & 0 & \frac{\partial}{\partial x} \\ 0 & \frac{\partial}{\partial z} & \frac{\partial}{\partial y} \end{bmatrix} \quad \overline{\overline{\mathbf{A}}} = \begin{bmatrix} \Delta u_{,x} & 0 & 0 & \Delta v_{,x} & 0 & 0 & \Delta w_{,x} & 0 & 0 \\ 0 & \Delta u_{,y} & 0 & 0 & \Delta v_{,y} & 0 & 0 & \Delta w_{,y} & 0 \\ 0 & 0 & \Delta u_{,z} & 0 & 0 & \Delta v_{,z} & 0 & 0 & \Delta w_{,z} \\ \Delta u_{,y} & \Delta u_{,x} & 0 & \Delta v_{,y} & \Delta v_{,x} & 0 & \Delta w_{,y} & \Delta w_{,x} & 0 \\ 0 & \Delta u_{,z} & \Delta u_{,y} & 0 & \Delta v_{,z} & \Delta v_{,y} & 0 & \Delta w_{,z} & \Delta w_{,y} \\ \Delta u_{,z} & 0 & \Delta u_{,x} & \Delta v_{,z} & 0 & \Delta v_{,x} & \Delta w_{,z} & 0 & \Delta w_{,x} \end{bmatrix} \tag{7}$$

Substituting the described relations, into the virtual work equation, Eqn 3, and assuming that the equation is precisely fulfilled at the end of the step we obtain the following incremental form of the virtual work equation

$$\int_{\Omega^t} \left({}_t^t\boldsymbol{\tau} \cdot \delta\boldsymbol{\eta} + \Delta\mathbf{S} \cdot \delta\Delta\mathbf{e} \right) d\Omega^t = \int_{\Omega^t} \Delta\mathbf{f}\, \delta\Delta\mathbf{u}\, d\Omega^t + \int_{\partial\Omega_\sigma^t} \Delta\mathbf{t}\, \delta\Delta\mathbf{u}\, d\left(\partial\Omega_\sigma^t\right) \tag{8}$$

Employing the finite element approximation $\Delta\mathbf{u} = \mathbf{N}\Delta\mathbf{q}$ and $\Delta\mathbf{u}' = \mathbf{B}_L'\Delta\mathbf{q}$, where $\mathbf{N}$ is the set of shape functions and $\Delta\mathbf{q}$ is the increment of nodal displacements and considering the following set of equalities

$${}_t^t\boldsymbol{\tau}^{\mathrm{T}}\delta\boldsymbol{\eta} = {}_t^t\boldsymbol{\tau}\delta\left(\overline{\overline{\mathbf{A}}}\right)\Delta\mathbf{u}' = \delta\left(\Delta\mathbf{u}'\right)^{\mathrm{T}}\, {}_t^t\overline{\boldsymbol{\tau}}\,\Delta\mathbf{u}' = \delta(\Delta\mathbf{q})^{\mathrm{T}}\, {}_t^t\overline{\boldsymbol{\tau}}\,\mathbf{B}_L' \tag{9}$$

where ${}_t^t\overline{\boldsymbol{\tau}}$ is the Cauchy stress matrix

$${}_t^t\overline{\boldsymbol{\tau}} = \begin{bmatrix} {}_t^t\underline{\boldsymbol{\tau}} & & \\ & {}_t^t\underline{\boldsymbol{\tau}} & \\ & & {}_t^t\underline{\boldsymbol{\tau}} \end{bmatrix} \quad {}_t^t\underline{\boldsymbol{\tau}} = \begin{bmatrix} {}_t^t\sigma_{xx} & {}_t^t\tau_{xy} & {}_t^t\tau_{xz} \\ & {}_t^t\sigma_{yy} & \tau_{yz} \\ & & {}_t^t\sigma_{zz} \end{bmatrix} \tag{10}$$

we obtain the following discretized form of the virtual work equation

$$\left(\int_{\Omega^t}\mathbf{B}_{\mathrm{L}}'^{\mathrm{T}}\,{}_t^t\overline{\boldsymbol{\tau}}\mathbf{B}_{\mathrm{L}}'\,d\Omega^t\right)\Delta\mathbf{q}+\int_{\Omega^t}\mathbf{B}_{\mathrm{L}}^{\mathrm{T}}\Delta\mathbf{S}\,d\Omega^t=\int_{\Omega^t}\mathbf{N}^{\mathrm{T}}\Delta\mathbf{f}\,d\Omega^t+\int_{\partial\Omega_\sigma^t}\mathbf{N}^{\mathrm{T}}\Delta\mathbf{t}\,d\left(\partial\Omega_\sigma^t\right) \tag{11}$$

Now, we will deal with the constitutive model and employ the linearized constitutive equation, in fact with the stress increment, $\Delta\mathbf{S}$.

Finite strains

When considering the finite strains effect [6], [7], the gradient $\mathbf{F}=\partial(\mathbf{X}+\mathbf{u})/\partial\mathbf{X}$ is decomposed into its elastic and plastic parts, $\mathbf{F}=\mathbf{F}^e\mathbf{F}^p$, Fig. 1c. To integrate the constitutive relations the deformation increment $\Delta\mathbf{D}$ is rotated to the un-rotated configuration by means of rotation matrix obtained from polar decomposition $\mathbf{F}=\mathbf{VR}=\mathbf{RU}$, $\Delta\mathbf{d}=\mathbf{R}_{n+1}^T\Delta\mathbf{D}\mathbf{R}_{n+1}$, then the radial return is performed and stresses are transformed to the Cauchy stresses at $n+1$, $\boldsymbol{\sigma}_{n+1}=\mathbf{R}_{n+1}\boldsymbol{\sigma}_{n+1}^u\mathbf{R}_{n+1}^T$. The stresses are integrated using the consistent tangent matrix [8] and the integration is done in the un-rotated configuration as for small strains.

Stress updating procedure

To integrate the constitutive relations we exploit the relations given above using the integration for the un-rotated configuration and the backward integration rule. The algorithm arises from the depicted above relations for rotated and un-rotated strain rates and Cauchy stresses. The outline of the integration scheme is given below.

- Compute deformation gradient

$$\mathbf{F}_{t+\Delta t}^i=\frac{\partial\left(\mathbf{X}+\mathbf{u}_{n+1}^i\right)}{\partial\mathbf{X}}$$

- Compute polar decomposition

$$\mathbf{F}_{t+\Delta t}^t=\mathbf{R}_{t+\Delta t}^t\mathbf{U}_{t+\Delta t}^i$$

- Compute deformation increment over the step

$$\Delta\boldsymbol{\varepsilon}^i=\mathbf{B}_{t+\Delta t}^t\left(\mathbf{u}_{t+\Delta t}^i\right)$$

- Now, we take the elements of the strain increment $\Delta\boldsymbol{\varepsilon}^i$ and obtain the $\Delta\mathbf{D}^i$ and perform rotation of the increment of spatial deformation to the un-rotated configuration

$$\Delta\mathbf{d}^i=\mathbf{R}_{t+\Delta t}^{i\mathrm{T}}\Delta\mathbf{D}^i\mathbf{R}_{t+\Delta t}^i$$

- Then, we perform integration of the small strains constitutive model using backward Euler integration rule (predictor - corrector) where the stresses depend on the history, this is reflected by the stresses at time t and internal variables $\boldsymbol{\alpha}_t$.

$$\boldsymbol{\sigma}_{t+\Delta t}^{u(i)}=\boldsymbol{\sigma}_{t+\Delta t}^{u(i)}\left(\boldsymbol{\sigma}_t,\boldsymbol{\alpha}_t,\Delta\mathbf{d}^i\right)$$

- Transform the stresses to the true Cauchy stresses at $t+\Delta t$.

$$\boldsymbol{\sigma}_{t+\Delta t} = \mathbf{R}_{t+\Delta t}\boldsymbol{\sigma}^{u}_{t+\Delta t}\mathbf{R}^{\mathrm{T}}_{t+\Delta t}$$

The integration in the un-rotated configuration is performed using a consistent tangent formulation, [8].

Constitutive model.
The constitutive model is the Gurson Tvergaard model [9-11] with the yield function as follows

$$F = \left(\frac{\sigma^{M}}{\bar{\sigma}}\right)^{2} + 2q_1 f \cosh\left(\frac{3q_2\sigma_m}{2\bar{\sigma}}\right) - \left(1+q_3 f^{2}\right) \tag{12}$$

where σ^{M} *is the Mises stress,* σ_m *is the mean stress,* $\bar{\sigma}$ *is the Mises stress in the matrix,* f *is the void ratio and* q_1, q_2, q_3 *are the Tvergaard coefficients.*

The stress integration algorithm comprises the elastic trial stress (predictor) and the corrector. It conforms the radial return algorithm. The algorithm can be derived basing on [12]. The elastic trial stress are of the form

$$\boldsymbol{\sigma}^{\mathrm{T}}_{m+1} = \boldsymbol{\sigma}_m + \mathbf{D}\ \Delta\boldsymbol{\varepsilon}^{pl} \tag{13}$$

The deviatioric and the volumetric stresses are of the form

$$q_{m+1} = \sqrt{\left(\frac{3}{2}S_{ij}S_{ij}\right)}_{m+1}; \qquad p_{m+1} = -\frac{1}{3}\left(\sigma_{11}+\sigma_{22}+\sigma_{33}\right)_{m+1} \tag{14}$$

The increment of the plastic strains can be obtained from the normality condition

$$d\boldsymbol{\varepsilon}^{pl} = d\lambda\frac{\partial F}{\partial \boldsymbol{\sigma}}; \tag{15}$$

Further, the plastic strains increment and the unit normal vector are of the form

$$\Delta\boldsymbol{\varepsilon}^{pl} = \Delta\lambda\left(-\frac{1}{3}\frac{\partial F}{\partial p}\mathbf{I} + \frac{\partial F}{\partial q}\mathbf{n}\right)_{m+1}; \qquad \mathbf{n}_{m+1} = \frac{3}{2q_{m+1}}\mathbf{S}_{m+1} \tag{16}$$

The volumetric and deviatoric plastic strains are as follows

$$\Delta\varepsilon^{pl}_{p} = -\Delta\lambda\left(\frac{\partial F}{\partial p}\right)_{m+1}, \qquad \Delta\varepsilon^{pl}_{q} = \Delta\lambda\left(\frac{\partial F}{\partial q}\right)_{m+1} \tag{17}$$

The stress at the end of the step after performing radial return

$$\boldsymbol{\sigma}_{m+1} = \boldsymbol{\sigma}^{\mathrm{T}} - \mathbf{D}\Delta\boldsymbol{\varepsilon}^{pl} \tag{18}$$

Since the increment of plastic strains is

$$\Delta\boldsymbol{\varepsilon}^{pl} = \frac{1}{3}\Delta\varepsilon_p \mathbf{I} + \Delta\varepsilon_q \mathbf{n}_{m+1} \tag{19}$$

the stress at the end of the step may be expressed as follows

$$\boldsymbol{\sigma}_{m+1} = \boldsymbol{\sigma}^{\mathrm{T}}_{m+1} - K\Delta\varepsilon_p \mathbf{I} - 2G\Delta\varepsilon_q \mathbf{n}_{m+1} \tag{20}$$

Finally the updated stresses are of the form

$$\boldsymbol{\sigma}_{m+1} = \boldsymbol{\sigma}^{\mathrm{T}}_{m+1} - K\Delta\varepsilon_p \mathbf{I} - \frac{3G\Delta\varepsilon_q}{q^{\mathrm{T}}_{m+1}} \mathbf{S}^{\mathrm{T}}_{m+1} \tag{21}$$

where the (T) indexed values are the trial stresses.

NUMERICAL RESULTS

The mechanical properties of the polycrystal consisting of elastic grains (tungsten carbide) and metallic interfaces (cobalt) are as follows: grains; Young's modulus $4.1\text{x}10^{11}$Pa and Poisson's ratio 0.25, interfaces: Young modulus $2.1\text{x}10^{11}$Pa, Poisson's ratio 0.235, yield limit $2.97\text{x}10^{11}$Pa and small hardening modulus $1.0\text{x}10^{6}$Pa. The dimensions of the sample are 100x100x10 μm. The scheme of the Representative Volume Element (RVE) is given in Fig. 2.

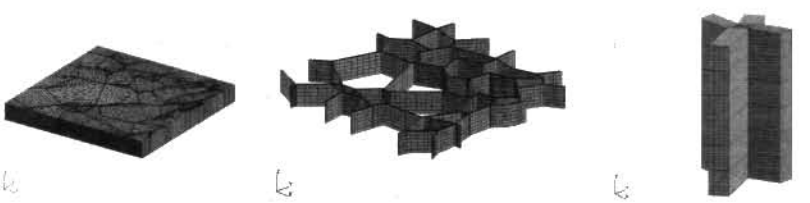

(a) (b) (c)

Figure 2. Mesh of representative volume element (a), interfaces (b), considered joint (c).

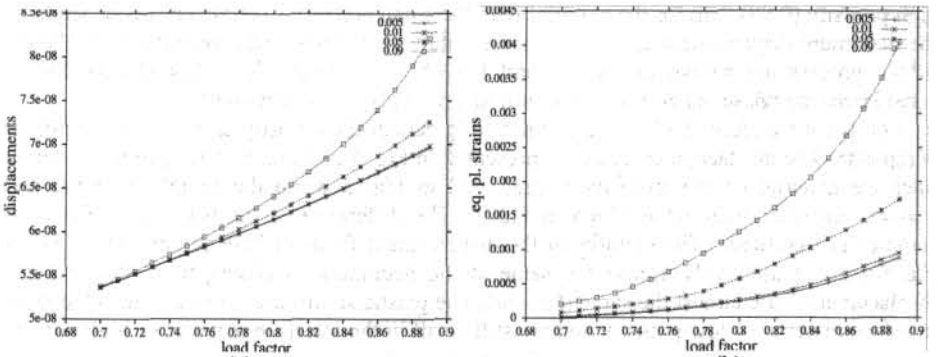

(a) (b)

Figure 3. Parametric study: porosity, displacements at the centre of the loaded face (a) and equivalent plastic strains in the considered joints (b) versus loading factor.

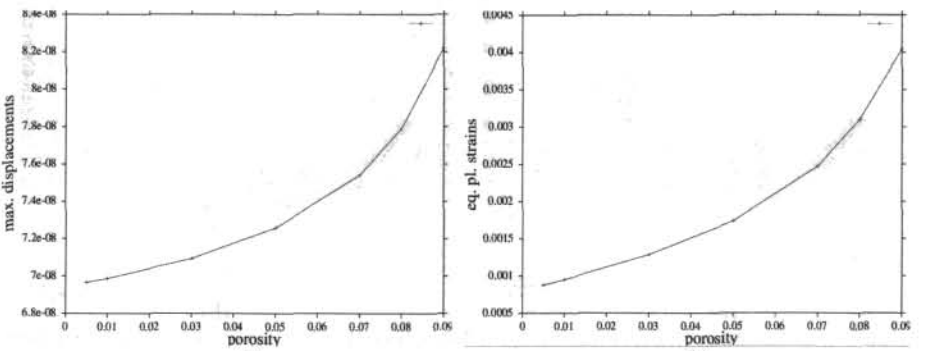

(a) (b)

Figure 4. Maximum displacement of the midpoint of the loaded face (a) and maximum equivalent plastic strain (b) in the considered interface joint.

The sample is discretized with 48894 elements and 58016 nodes. The sample is fixed on one side and loaded with the uniform pressure of 400 MPa on the other one. There is imposed symmetry condition in the bottom of the sample. Since the grains are elastic the sample fails due to large plastic strains occurring in the elasto-plastic interfaces, in particular in joints [13, 14]. However, in this case, we focus our attention on the additional deformation and additional plastic strains occurring in the interfaces due to existence of initial porosity therein. We will consider a "control node" at the midpoint of loaded face of the sample and a joint between 4 grains (Fig. 2b and Fig. 2c) where the plastic strains start to appear early.

The sample is loaded until 89% of the total load. The parametric study is performed for the values of porosity in the interfaces such as: 0.005, 0.01, 0.05, 0.09 (Fig. 3). The displacements and plastic strains strongly depend on the porosity of the material. This is presented in Fig. 3 and Fig. 4. We start to follow the equilibrium path at 70% of the total load when the plastic strains begin to develop for lowest value of porosity. The horizontal displacement of the chosen node increases nonlinearly and at the end of the process (89% of the total load), for porosity 0.09 is 15.3% higher than for the material with porosity 0.005. The dependence of the plastic strains development in the chosen joint on the porosity of the material is dramatically strong. The equivalent plastic strains are 362% higher for the material with the

high porosity (0.09) then for the material with the small porosity (0.005). The dependences of the maximum displacement and the maximum equivalent plastic strain on porosity at the end of the process are shown in Fig. 4a and Fig 4b, respectively. The dependences for the considered two-phase material are nonlinear and strongly dependent on porosity.

Let us have a closer look at the qualitative effects of the porosity on the behaviour of the composite. The displacement fields are presented in Fig. 5 and Fig. 6. The sample containing interface material of low porosity is presented in Fig. 5 while the sample with the high porosity interface material is given in Fig. 6. The difference of the behaviour of the two samples is significant. The pictures of the displacement fields of both samples (Fig. 5a and Fig 5b) are qualitatively almost the same at the beginning of observations. The "control displacements" are almost the same (Fig. 3a). The plastic strains are starting to develop in the interface material of low porosity and are still small in the interface material of high porosity (Fig. 3b). When observing the surface of the samples (Fig. 5a and Fig. 6a) we may notice only spots of plastic strains.

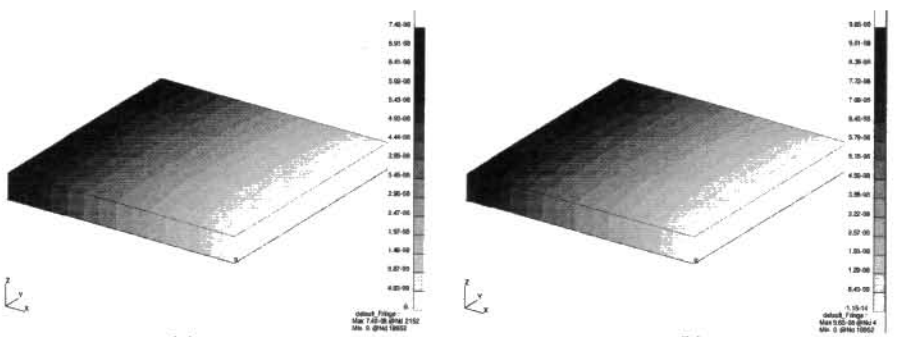

(a) (b)

Figure 5. Displacement fields at load factor 0.7 (a) and at load factor 0.89 (b), porosity 0.005.

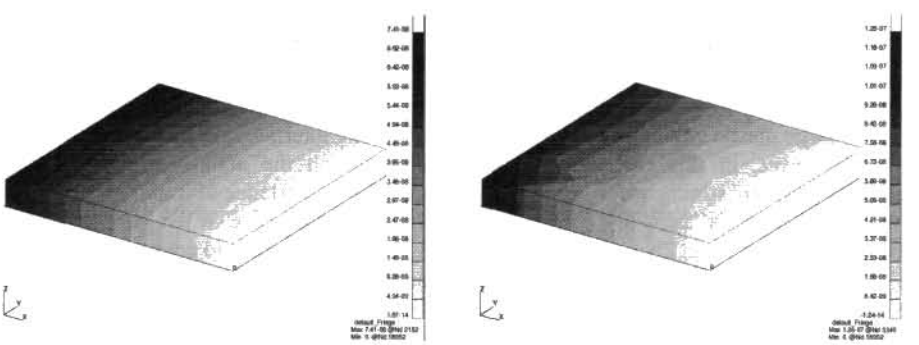

(a) (b)

Figure 6. Displacement fields at load factor 0.7 (a) and at load factor 0.89 (b), porosity 0.09.

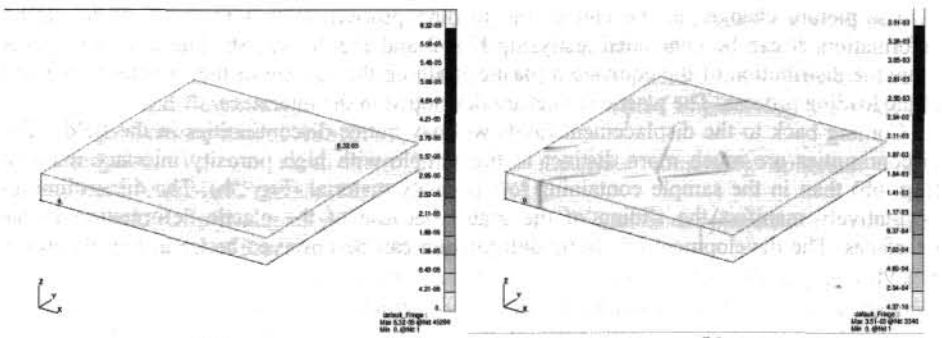

(a) (b)

Figure 7.Equivalent plastic strain distribution at load factor 0.7 (a) and at load factor 0.89 (b), porosity 0.005.

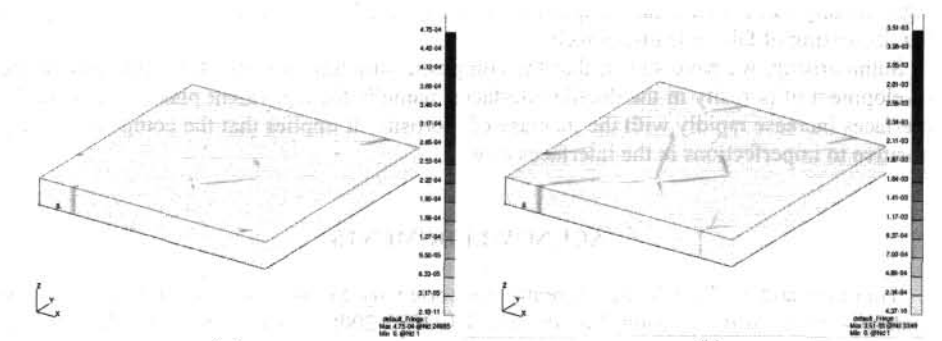

(a) (b)

Figure 8.Equivalent plastic strain distribution at load factor 0.7 (a) and at load factor 0.89 (b), porosity 0.09.

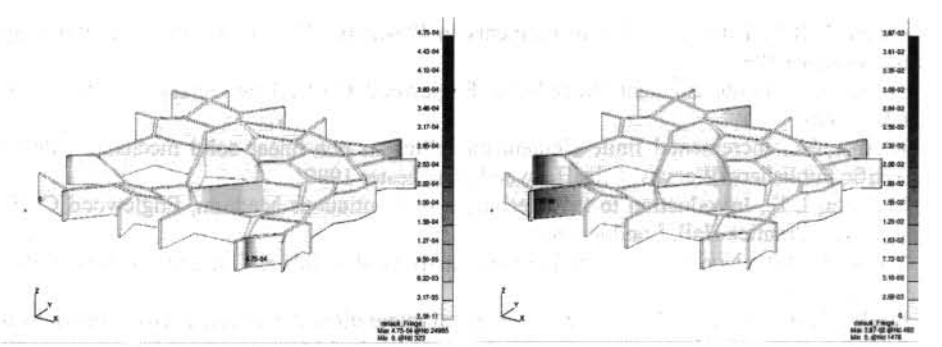

Figure 9. Equivalent plastic strain distribution in the interface at load factor 0.7 (a) and at load factor 0.89 (b), porosity 0.09.

The picture changes at the end of the loading process. Both samples undergo plastic deformation. It can be concluded analysing Fig. 3 and Fig 7b and 8b. The last two figures show the distribution of the equivalent plastic strain on the surface of the samples at the end of the loading process. The plastic strains are developed in the interfaces.

Coming back to the displacement fields we may notice discontinuities in the fields. The discontinuities are much more distinct in the sample with high porosity interface material (Fig. 6b) than in the sample containing low porosity material (Fig. 5b). The discontinuities qualitatively manifest the sliding of the grains because of the plastic deformation in the interfaces. The development of plastic deformation can be observed better in Fig .9a and in Fig. 9b.

FINAL REMARKS

The influence of porosity of the interfaces material was investigated. It has been found that the behaviour of the two-phase composite strongly depends on the porosity of interfaces in the material. Amount of porosity changes the qualitative behaviour of the two-phase material. High porosity values cause earlier appearance of the slips in the interfaces and it is anticipated that decreasing of failure loads, as well.

Summarising, we have shown that the composite structure is particularly sensitive to the development of porosity in the ductile interfaces, namely, the equivalent plastic strains in the interfaces increase rapidly with the increase of porosity. It implies that the composite is very sensitive to imperfections in the interfaces as well.

ACKNOWLEDGMENTS

T. Sadowski and E. Postek are currently supported by Polish Ministry of Education and Science - grant SPB, decision No 65/6.PR UE/2005-2008/7. The support of the Civil & Computational Engineering Centre at UWS is appreciated.

REFERENCES

1. Owen, D.R.J., Hinton, E., Finite Elements in Plasticity: Theory and Practice, Pineridge Press, Swansea 1980
2. Bathe, K.J., Finite Element Procedures, Englewood Cliffs, New Jersey, Prentice Hall, London 1996
3. Kleiber, M., Incremental finite element modelling in non-linear solid mechanics, Polish Scientific Publishers, Warsaw, Ellis Horwood, Chichester 1989.
4. Malvern, L.E., Introduction to the Mechanics of Continuous Medium, Englewood Cliffs, New Jersey, Prentice Hall, London 1969.
5. Crisfield, M.A., Non-linear Finite Element Analysis of Solids and Structures, John Wiley, New York 1991.
6. Pinsky, P.M., Ortiz, M., Pister, K.S., Numerical integration of rate constitutive equations in finite deformations analysis, Computer Methods in Applied Mechanics and Engineering, 40, 1983, pp. 137-158
7. Peric, D., Owen D.R.J., Honnor, M.E. A model for finite strain elasto-plasticity based on logarithmic strains: Computational issues, Computer Methods in Applied Mechanics and Engineering, 94, 1985, pp. 101-118

8. Simo, J.C., Taylor, R.L., Consistent tangent operators for rate independent elastoplasticity, Computer Methods in Applied Mechanics and Engineering, 48, 1985, pp. 101-118
9. Gurson, L., Continuum theory of ductile rupture by void nucleation and growth: part I - yield criteria and flow rules for porous ductile media, Journal of Engineering Materials and Technology, Transactions of ASME, 99, 1977, pp. 2-15
10. Tvergaard, V., On localization in ductile materials containing spherical voids, International Journal of Fracture, 18, 1982, pp. 237-252
11. Tvergaard, V., Influence of voids on shear-band instabilities under plane strain conditions, International Journal of Fracture, 17, 1981, pp. 389-407
12. Simo, J.C., Hughes, T.J.R., Computational Inelasticity, Springer, New York-London 1998
13. Postek, E., Sadowski, T., Hardy, S.J., The mechanical response of a ceramic polycrystalline material with inter-granular layers. In: Proc. "VIII International Conference on Computational Plasticity, COMPLAS VIII", E. Oñate, D.R.J. Owen eds. Barcelona Sept. 2005, CIMNE Barcelona 2005
14. Sadowski, T., Hardy S., Postek, E., A new model for the time-dependent of polycrystalline ceramic materials with metallic inter-granular layers under tension, Material Science and Engineering A, 2006, pp. 230-238